Electronic Supplementary Material (ESI) for Polymer Chemistry.

Electronic Supplementary Information

Synthesis of platinum(II) complex end functionalized star polymers: Luminescence enhancements and unimolecular micelles in solvents of weakened quality

Fang Qu, Beihong Yang, Qun He, and Weifeng Bu*

Key Laboratory of Nonferrous Metals Chemistry and Resources Utilization of Gansu Province, State Key Laboratory of Applied Organic Chemistry, and College of Chemistry and Chemical Engineering, Lanzhou University, Lanzhou City, Gansu Province, China, E-mail: buwf@lzu.edu.cn

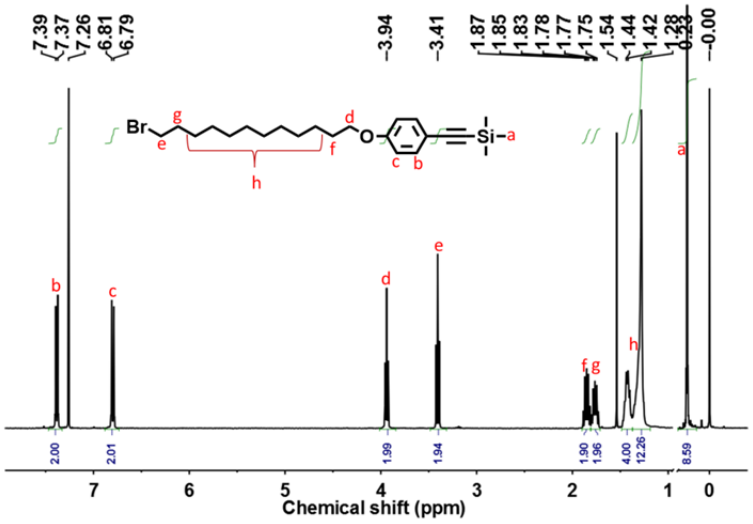

Fig. S1 ^{1}H NMR spectrum of **2** in $CDCl_3$.

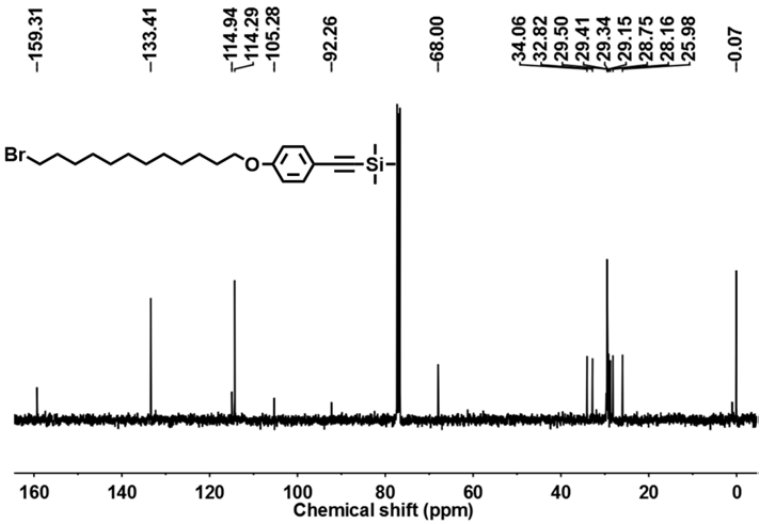

Fig. S2 ^{13}C NMR spectrum of **2** in $CDCl_3$.

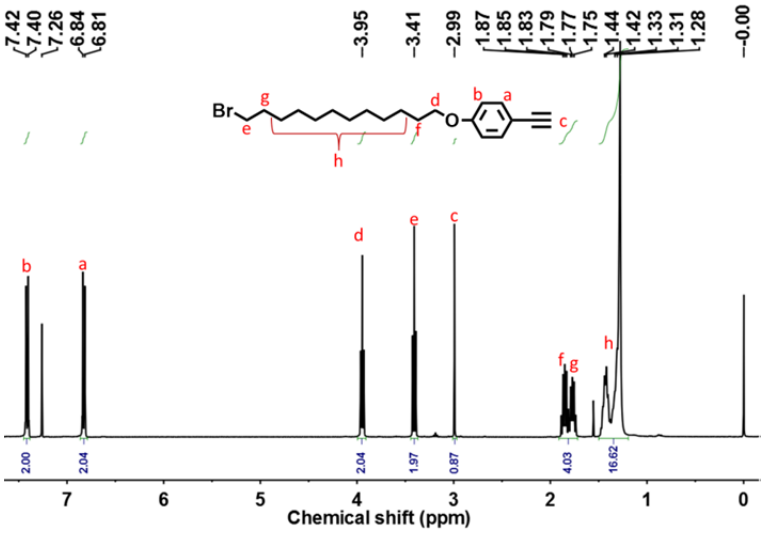

Fig. S3 ^{1}H NMR spectrum of **3** in $CDCl_3$.

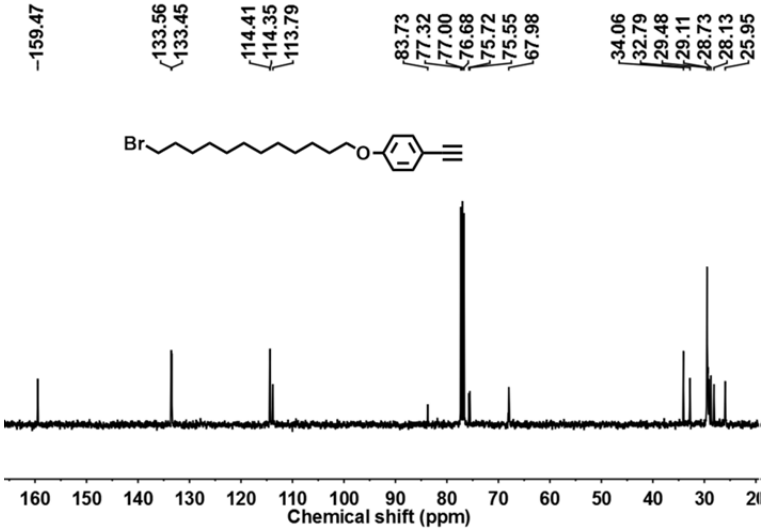

Fig. S4 ^{13}C NMR spectrum of **3** in $CDCl_3$.

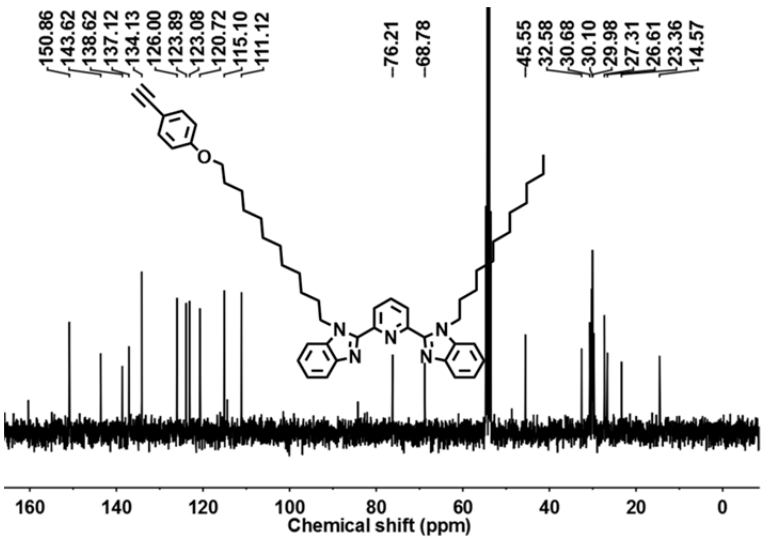

Fig. S5 ^{13}C NMR spectrum of **5** in CD_2Cl_2.

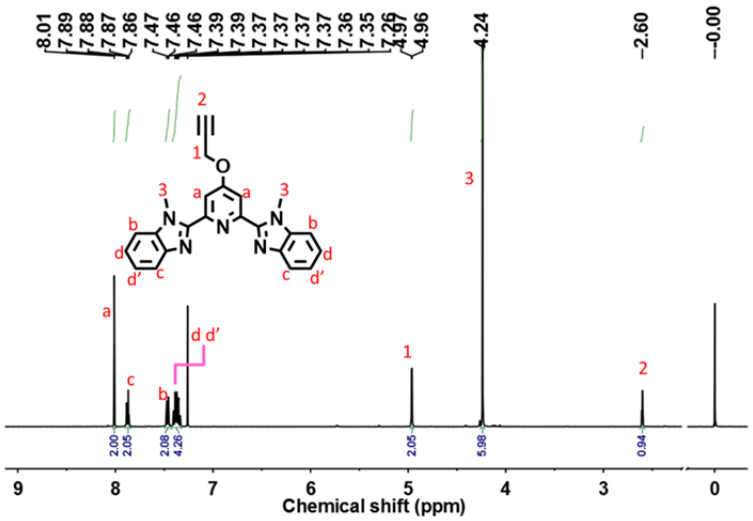

Fig. S6 ^{13}H NMR spectrum of **7** in $CDCl_3$.

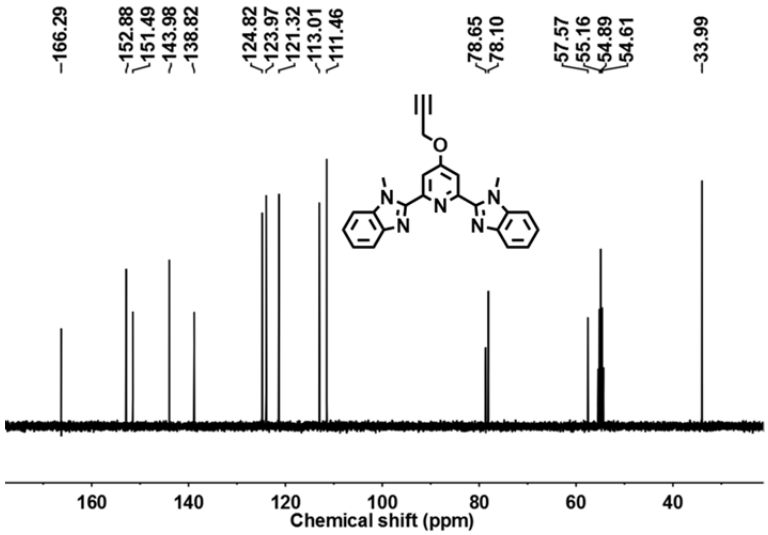

Fig. S7 ^{13}C NMR spectrum of **7** in CD_2Cl_2.

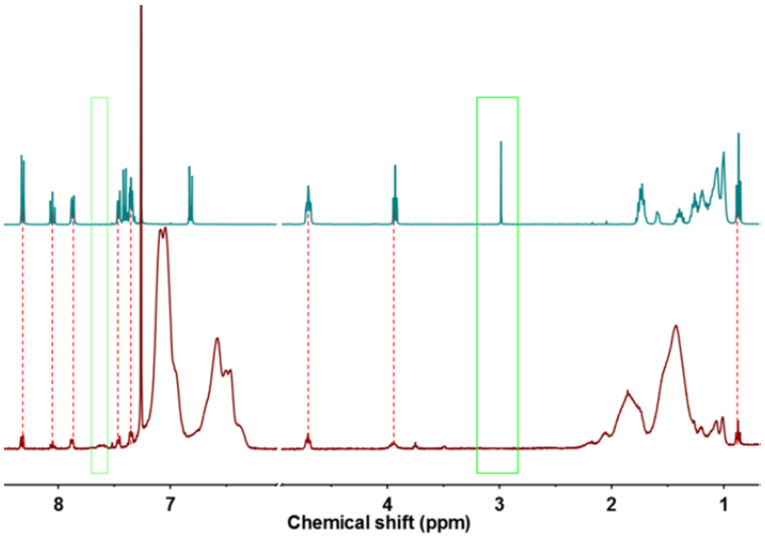

Fig. S8 ^{1}H NMR spectra of **5** (Top) and **SS$_{61}$L-I** (Bottom) in $CDCl_3$.

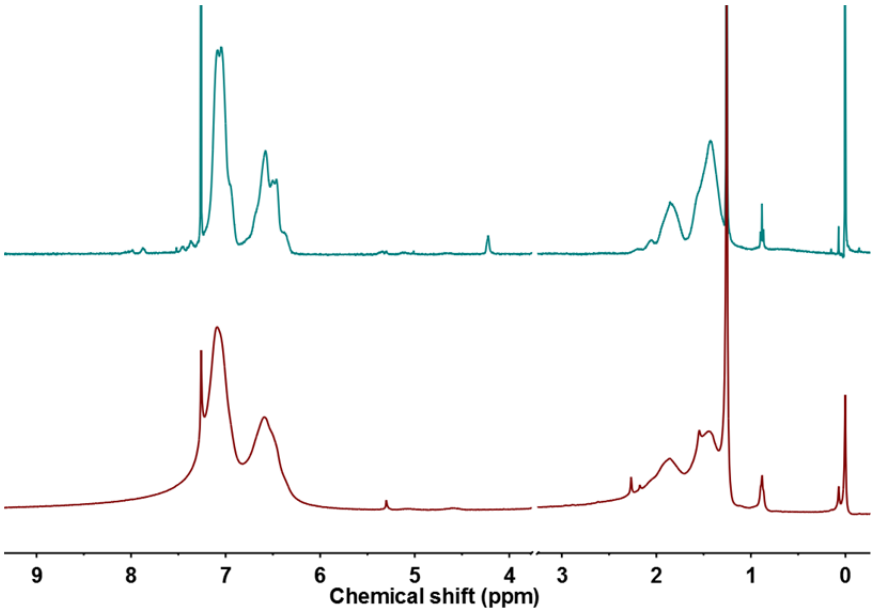

Fig. S9 ^{1}H NMR spectra of **SS$_{61}$L-II** (Top) and **SS$_{61}$Pt-II** (Bottom) in $CDCl_3$. **SS$_{61}$L-II** was obtained as a white solid with a similar yield of 91% on the basis of **SS$_6$N$_3$**, where the click modification is sufficient. In the case of **SS$_{61}$L-I**, the bzimpy ligand are connected with alkyl chains. The difference is that there is no alkyl chains in **SS$_{61}$L-II**. Therefore, the former star ligand occupied a much larger solubility and mobility in $CHCl_3$ than the latter, leading to the presence of much more pronounced resonance signals in the former case. Alternatively, the end ligands of **SS$_{61}$L-II** were more easily encapsulated into the star polystyrene than those of **SS$_{61}$L-I**. In addition, 2,6-bis(*N*-methylbenzimidazol-2′-yl)pyridine, the end ligand of **SS$_{61}$L-II**, showed a limited solubility in $CHCl_3$ and aggregated there. Therefore, **SS$_{61}$L-II** showed a much easier tendency to form aggregates in $CHCl_3$. Accordingly, it is not strange that the ^{1}H NMR signals of the ligand are very weak for **SS$_{61}$L-II** compared to **SS$_{61}$L-I**.

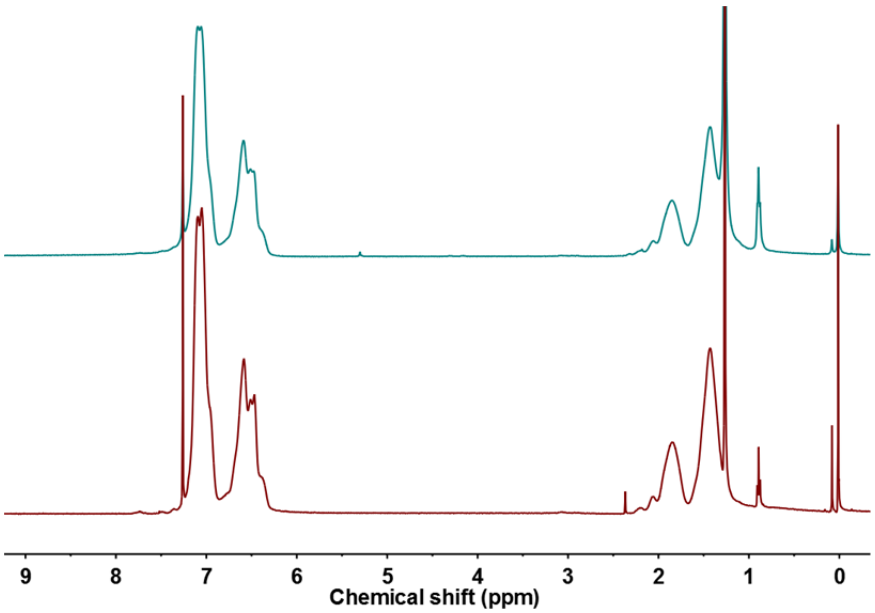

Fig. S10 ^{1}H NMR spectra of **SS$_{101}$L-II** (Top) and **SS$_{101}$Pt-II** (Bottom) in $CDCl_3$.

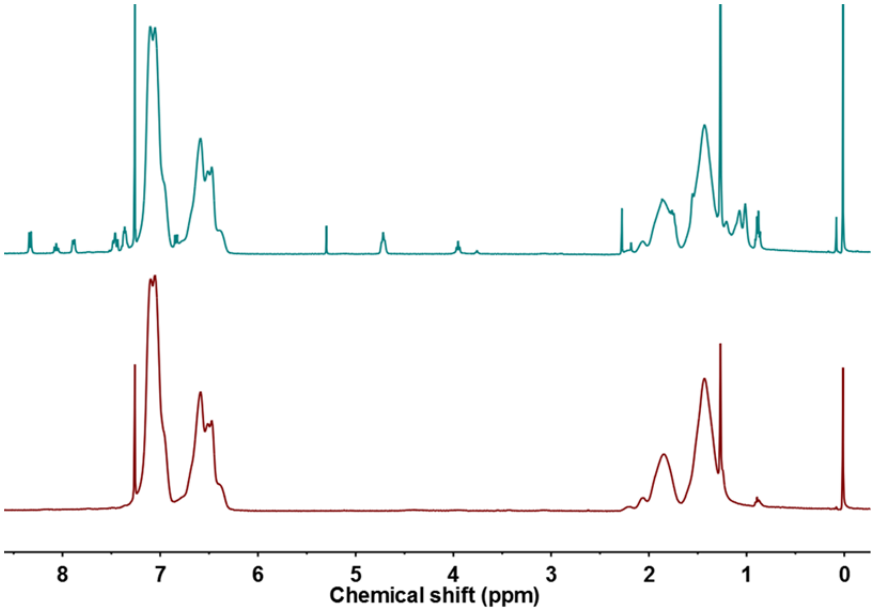

Fig. S11 ^{1}H NMR spectra of **SS$_{152}$L-I** (Top) and **SS$_{152}$Pt-I** (Bottom) in $CDCl_3$. It is true that the end ligands of the star polymers are diluted for the species with higher molecular weight. However, in the starlike polymers, the local density of the end ligand increased with the decreasing molecular weight. Here, the maximum ligand density was achieved at **SS$_{61}$L-I**. Therefore, the star of **SS$_{61}$L-I** was more inclined to aggregate in $CHCl_3$ than that of **SS$_{152}$L-I**. On the other hand, with the increasing molecular weight, the end ligands were totally exposed in the solvent environment. These features lead to sharper resonance signals of **SS$_{152}$L-I**.

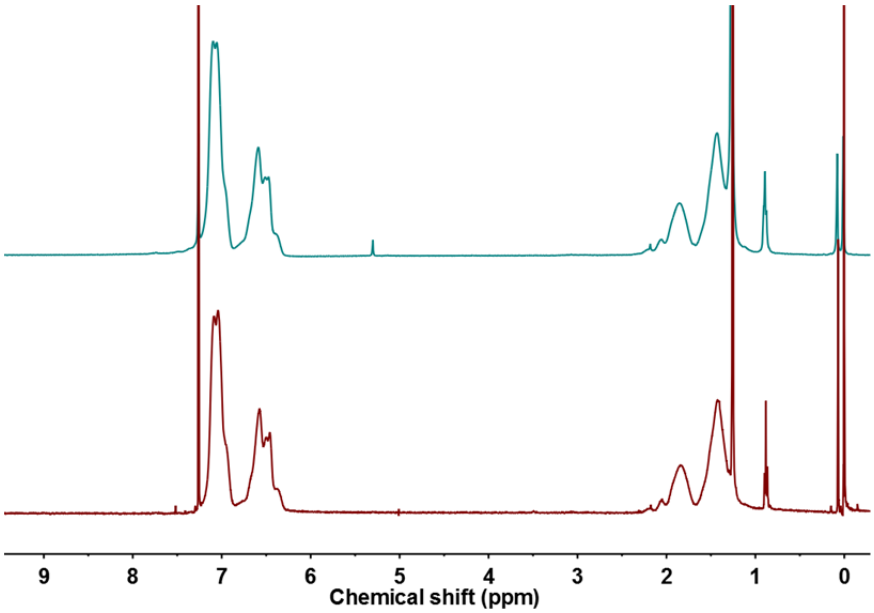

Fig. S12 ^{1}H NMR spectra of **SS$_{152}$L-II** (Top) and **SS$_{152}$Pt-II** (Bottom) in $CDCl_3$.

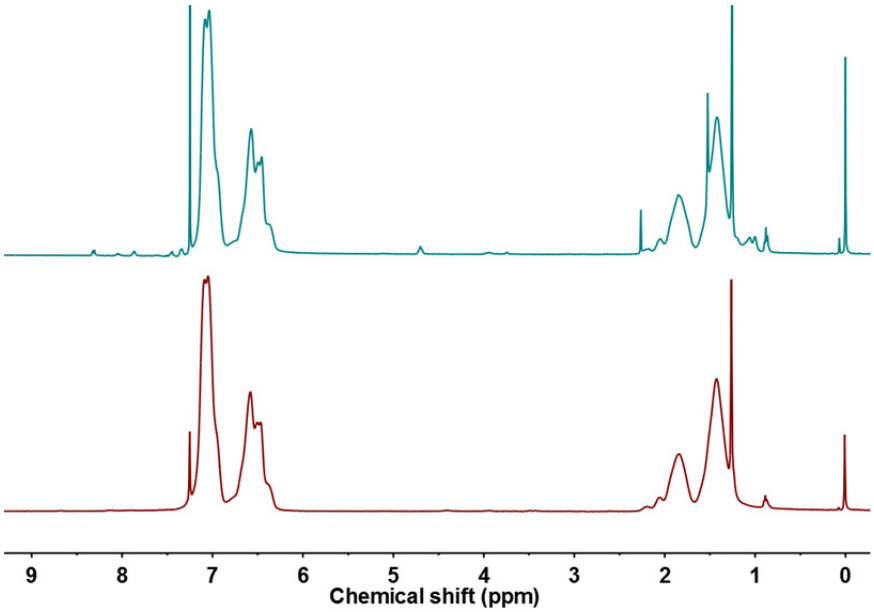

Fig. S13 ^{1}H NMR spectra of **SS$_{274}$L-I** (Top) and **SS$_{274}$Pt-I** (Bottom) in $CDCl_3$.

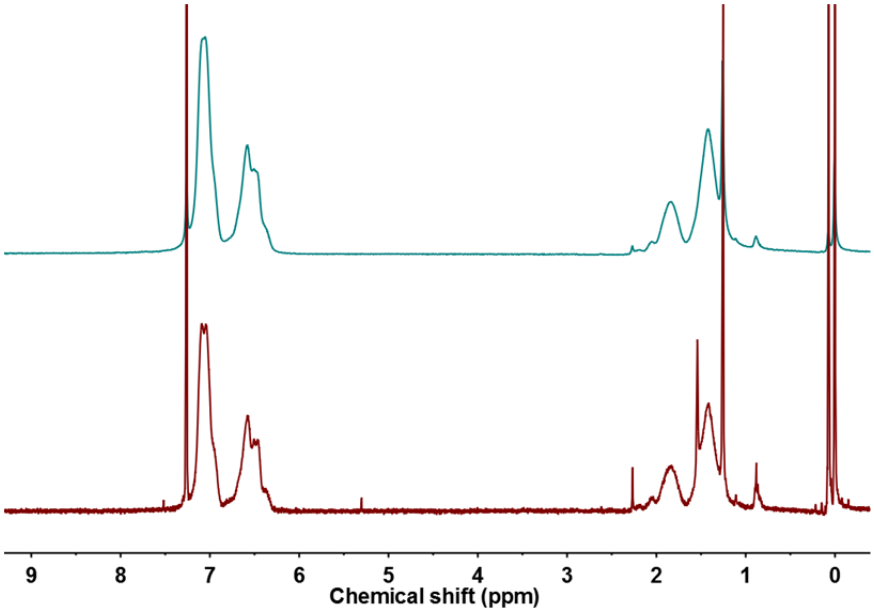

Fig. S14 ^{1}H NMR spectra of **SS$_{274}$L-II** (Top) and **SS$_{274}$Pt-II** (Bottom) in $CDCl_3$.

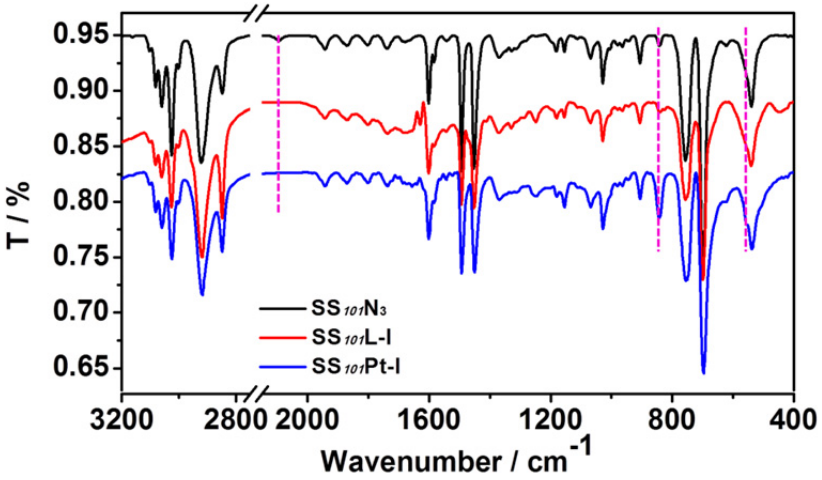

Fig. S15 FT-IR spectra of **$SS_{101}N_3$**, **SS_{101}L-I**, and **SS_{101}Pt-I**.

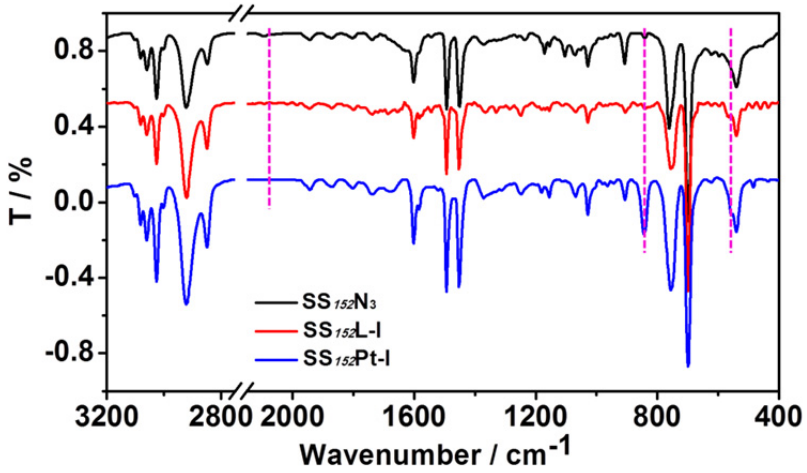

Fig. S16 FT-IR spectra of **$SS_{152}N_3$**, **SS_{152}L-I**, and **SS_{152}Pt-I**.

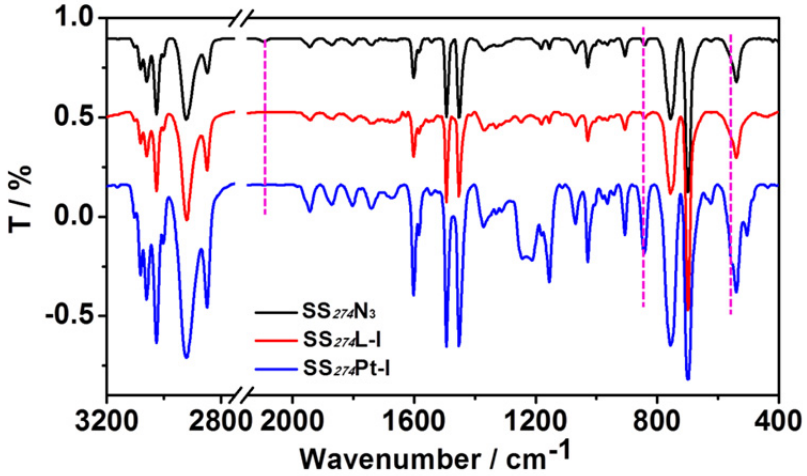

Fig. S17 FT-IR spectra of **$SS_{274}N_3$**, **SS_{274}L-I**, and **SS_{274}Pt-I**.

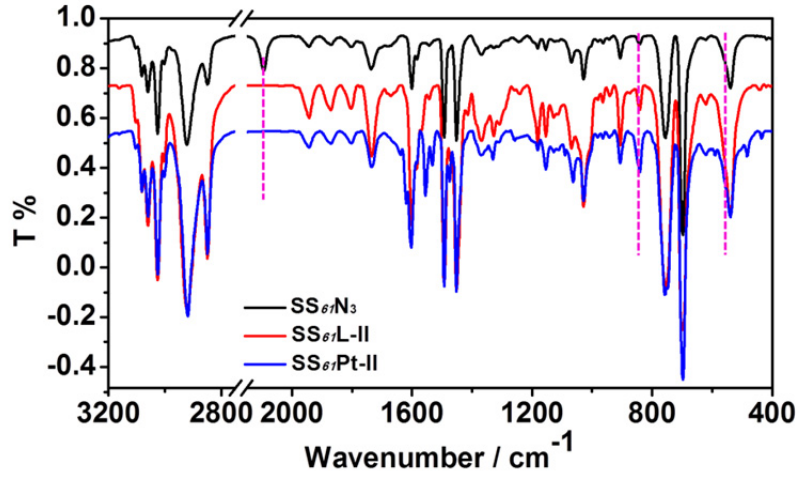

Fig. S18 FT-IR spectra of **$SS_{61}N_3$**, **SS_{61}L-II**, and **SS_{61}Pt-II**.

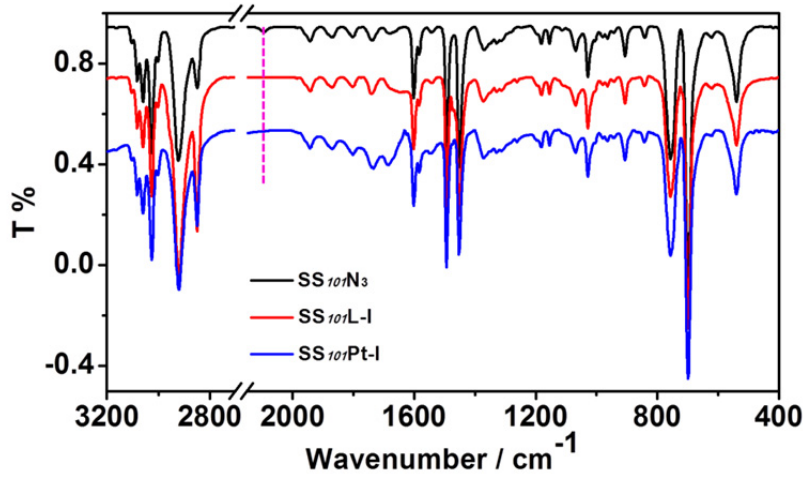

Fig. S19 FT-IR spectra of **$SS_{101}N_3$**, **SS_{101}L-II**, and **SS_{101}Pt-II**.

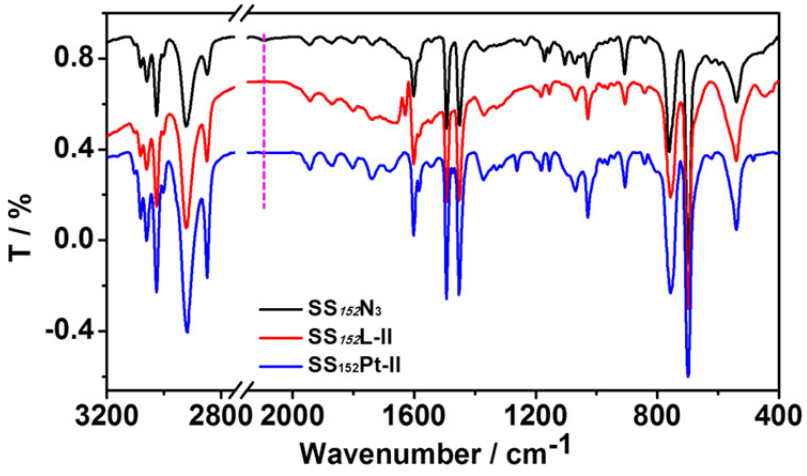

Fig. S20 FT-IR spectra of **$SS_{152}N_3$**, **SS_{152}L-II**, and **SS_{152}Pt-II**.

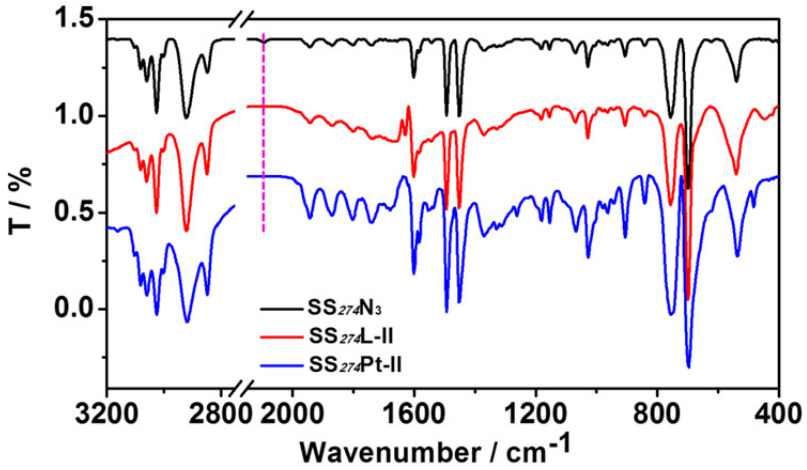

Fig. S21 FT-IR spectra of **$SS_{274}N_3$**, **SS_{274}L-II**, and **SS_{274}Pt-II**.

Table. S1 Elemental Analyses Established Compositions of Platinum(II) Complex End Functionalized Star Polymers

Sample Chemical Formula	Calculated			Found		
	C	H	N	C	H	N
SS_{61}-Pt-I $C_{126}H_{175}O_{56}[(C_8H_8)_{61}C_{51}H_{65}N_8OPtClPF_6(H_2O)_3]_{21}$	84.93	7.35	0.98	84.49	7.49	0.31
SS_{101}-Pt-I $C_{126}H_{175}O_{56}[(C_8H_8)_{101}C_{51}H_{65}N_8OPtClPF_6(H_2O)_9]_{21}$	86.72	7.36	0.94	86.13	7.16	0.55
SS_{152}-Pt-I $C_{126}H_{175}O_{56}[(C_8H_8)_{152}C_{51}H_{65}N_8OPtClPF_6(H_2O)]_{21}$	89.18	7.52	0.65	89.07	6.89	0.38
SS_{274}-Pt-I $C_{126}H_{175}O_{56}[(C_8H_8)_{274}C_{51}H_{65}N_8OPtClPF_6(H_2O)_3]_{21}$	92.63	6.84	0.29	92.37	7.39	0.98
SS_{61}-Pt-II $C_{126}H_{175}O_{56}[(C_8H_8)_{61}C_{24}H_{19}N_8OPtClPF_6(H_2O)_{20}]_{21}$	81.38	7.27	1.47	80.96	7.14	1.52
SS_{101}-Pt-II $C_{126}H_{175}O_{56}[(C_8H_8)_{101}C_{24}H_{19}N_8OPtClPF_6(H_2O)_4]_{21}$	87.37	7.26	0.97	87.01	7.91	0.19
SS_{152}-Pt-II $C_{126}H_{175}O_{56}[(C_8H_8)_{152}C_{24}H_{19}N_8OPtClPF_6(H_2O)_{14}]_{21}$	87.99	7.48	0.66	87.45	7.88	0.32
SS_{274}-Pt-II $C_{126}H_{175}O_{56}[(C_8H_8)_{274}C_{24}H_{19}N_8OPtClPF_6(H_2O)_{10}]_{21}$	90.05	7.56	0.38	89.80	7.64	0.31

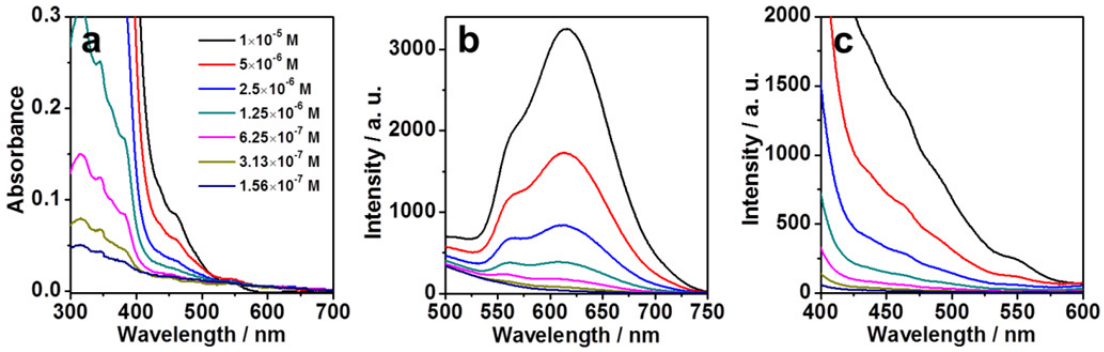

Fig. S22 UV-vis absorption (a), emission (b), and exitation spectra (c) of **SS$_{61}$Pt-I** in chloroform with the increasing concentration.

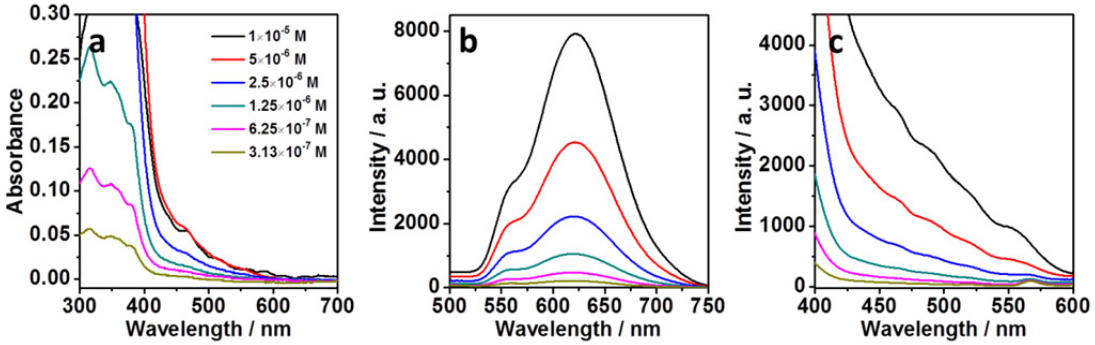

Fig. S23 UV-vis absorption (a), emission (b), and exitation spectra (c) of **SS$_{152}$Pt-I** in toluene with the increasing concentration.

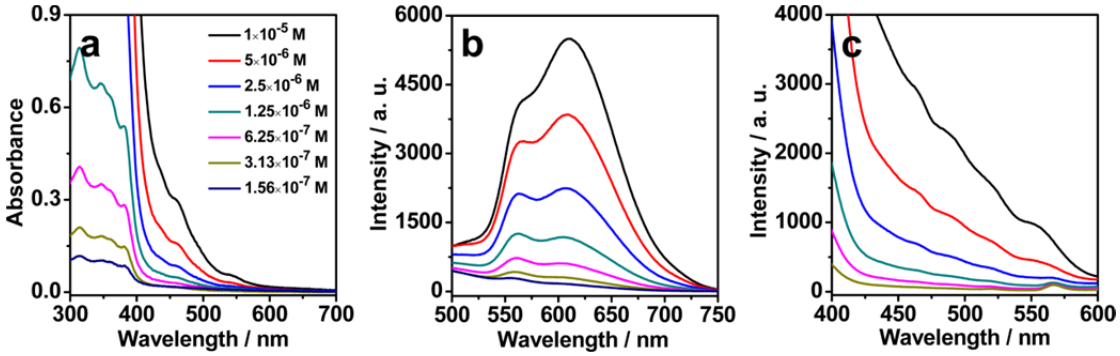

Fig. S24 UV-vis absorption (a), emission (b), and exitation spectra (c) of **SS$_{152}$Pt-I** in chloroform with the increasing concentration.

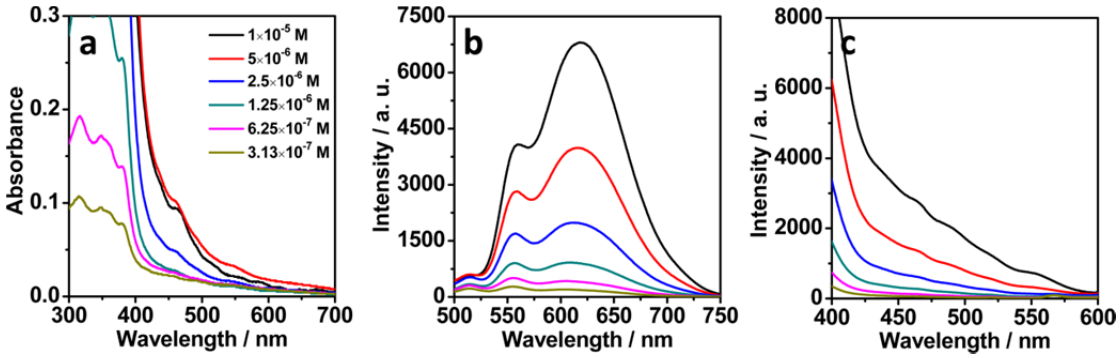

Fig. S25 UV-vis absorption (a), emission (b), and exitation spectra (c) of **SS$_{274}$Pt-I** in toluene with the increasing concentration.

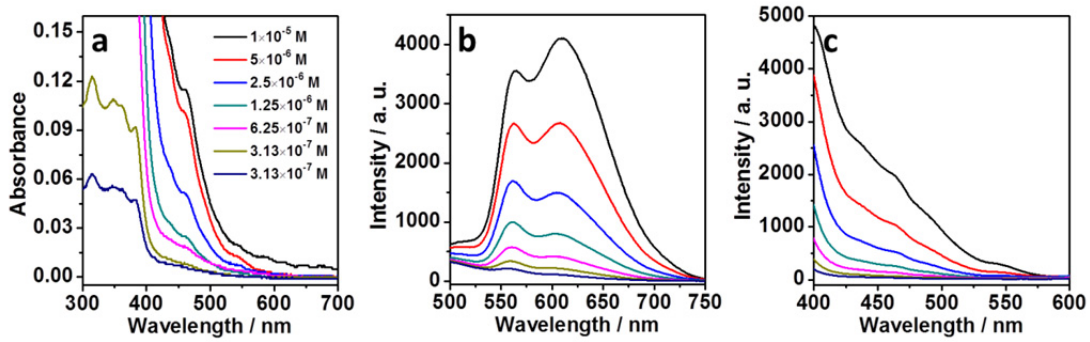

Fig. S26 UV-vis absorption (a), emission (b), and exitation spectra (c) of **SS$_{274}$Pt-I** in chloroform with the increasing concentration.

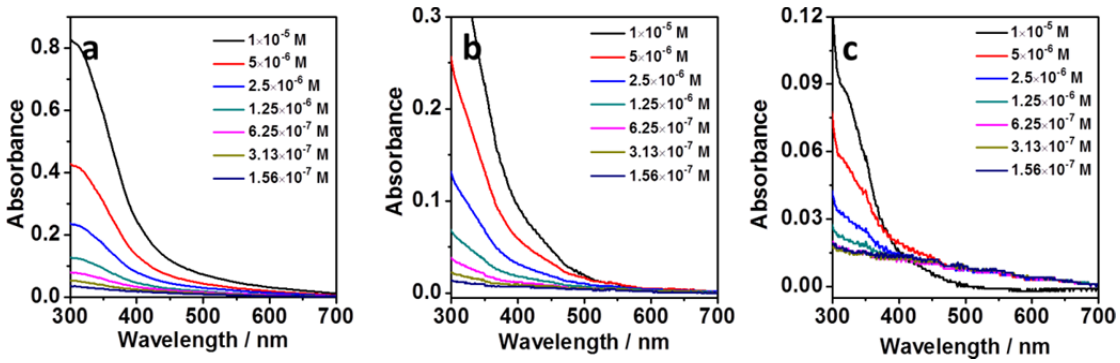

Fig. S27 UV-vis absorption spectra of **SS$_{101}$Pt-II** (a), **SS$_{152}$Pt-II** (b), and **SS$_{274}$Pt-II** (c) in toluene with the increasing concentration.

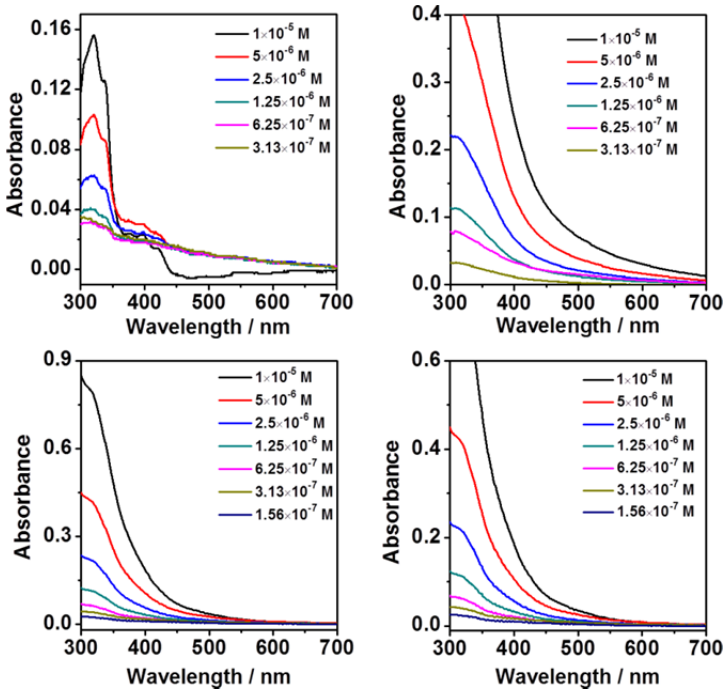

Fig. S28 UV-vis absorption spectra of **SS$_{61}$Pt-II** (a), **SS$_{101}$Pt-II** (b), **SS$_{152}$Pt-II** (c), and **SS$_{274}$Pt-II** (d) in chloroform with the increasing concentration.

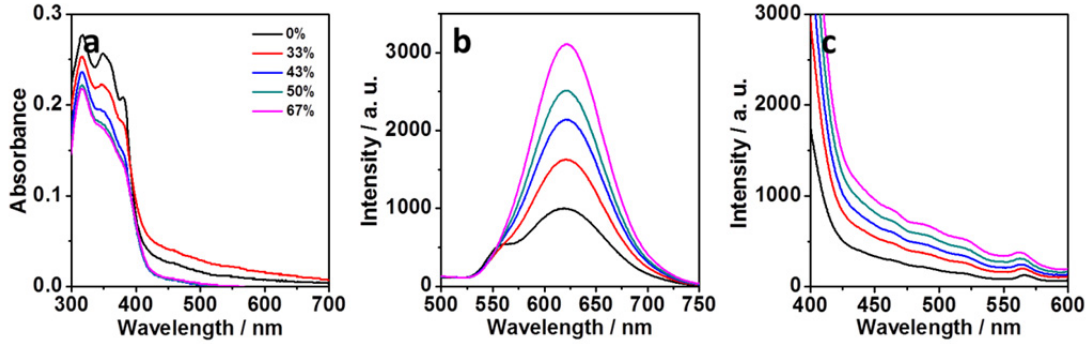

Fig. S29 UV-vis absorption (a), emission (b), and exitation spectra (c) of **SS$_{152}$Pt-I** dispersed in the toluene/*n*-hexane mixture solvents.

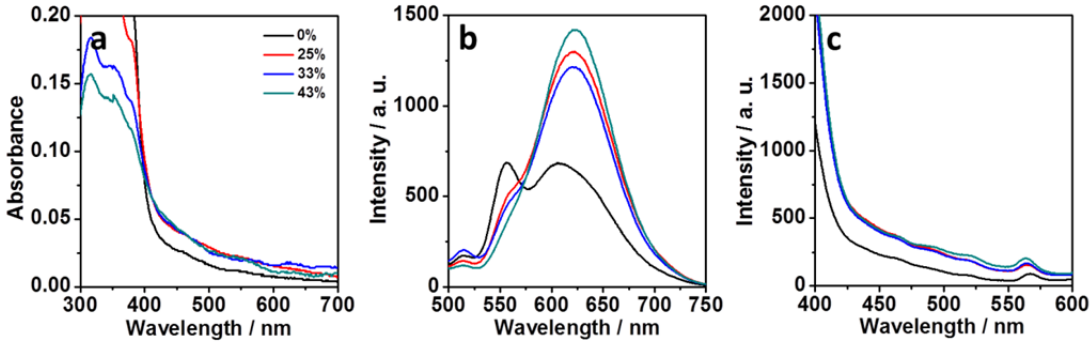

Fig. S30 UV-vis absorption (a), emission (b), and exitation spectra (c) of **SS$_{274}$Pt-I** dispersed in the toluene/*n*-hexane mixture solvents. Because of the large molecular weight, **SS$_{274}$Pt-I** started to precipitate even at the *n*-hexane content of 50%.

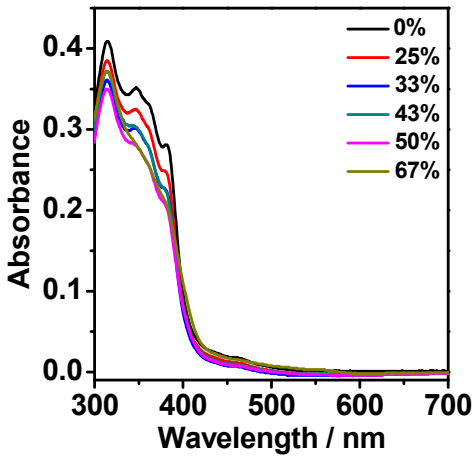

Fig. S31 UV-vis absorption spectra of **SS$_{152}$Pt-I** in the chloroform/*n*-hexane mixture solvents.

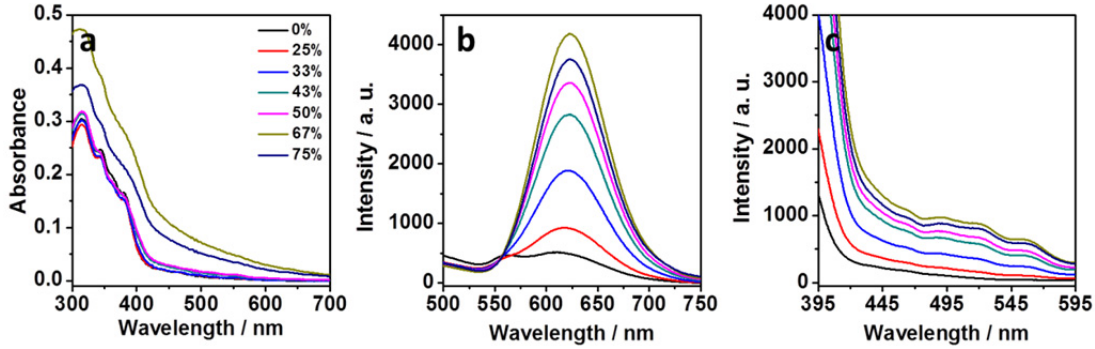

Fig. S32 UV-vis absorption (a), emission (b), and exitation spectra (c) of **SS$_{61}$Pt-I** dispersed in the chloroform/*n*-hexane mixture solvents.

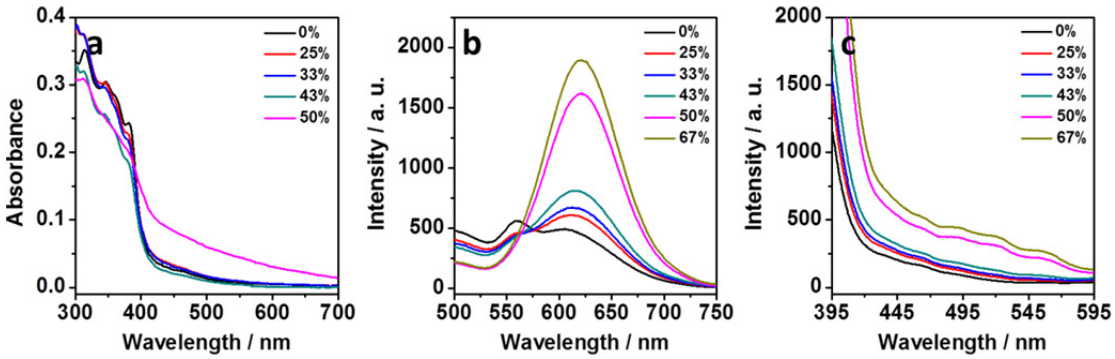

Fig. S33 UV-vis absorption (a), emission (b), and exitation spectra (c) of **SS$_{101}$Pt-I** dispersed in the chloroform/*n*-hexane mixture solvents.

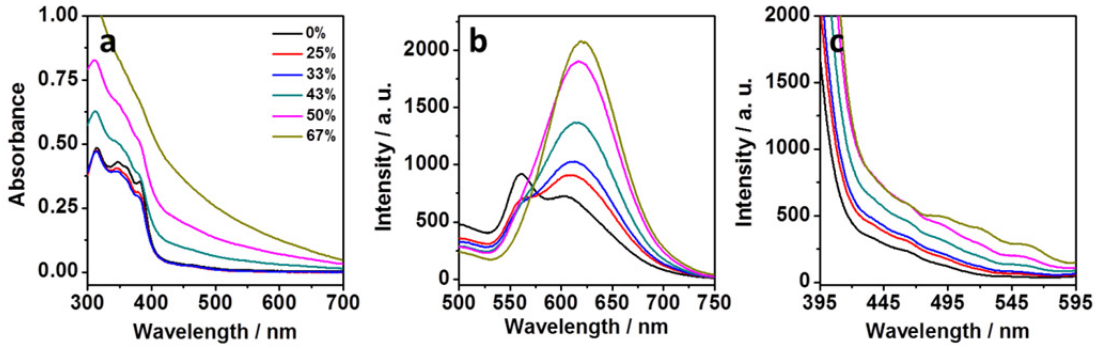

Fig. S34 UV-vis absorption (a), emission (b), and exitation spectra (c) of **SS$_{274}$Pt-I** dispersed in the chloroform/*n*-hexane mixture solvents.

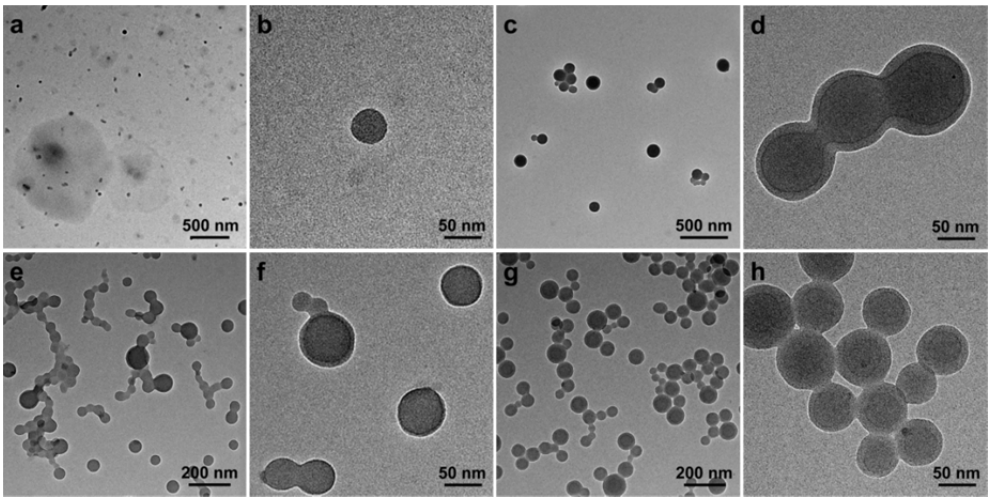

Fig. S35 TEM images of **SS$_{61}$Pt-II** (a and b), **SS$_{101}$Pt-II** (c and d), **SS$_{152}$Pt-II** (e and f) and **SS$_{274}$Pt-I** (g and h) obtained respectively from their chloroform/methanol solvents with a methanol volume ratio of 90%.

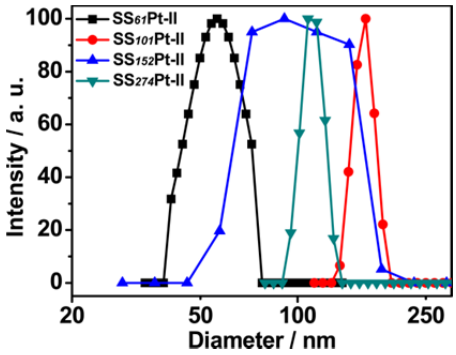

Fig. S36 DLS plots of **SS$_{61}$Pt-II**, **SS$_{101}$Pt-II**, **SS$_{152}$Pt-II**, and **SS$_{274}$Pt-II** dispersed in the chloroform/methanol solvent with a methanol volume ratio of 90%.

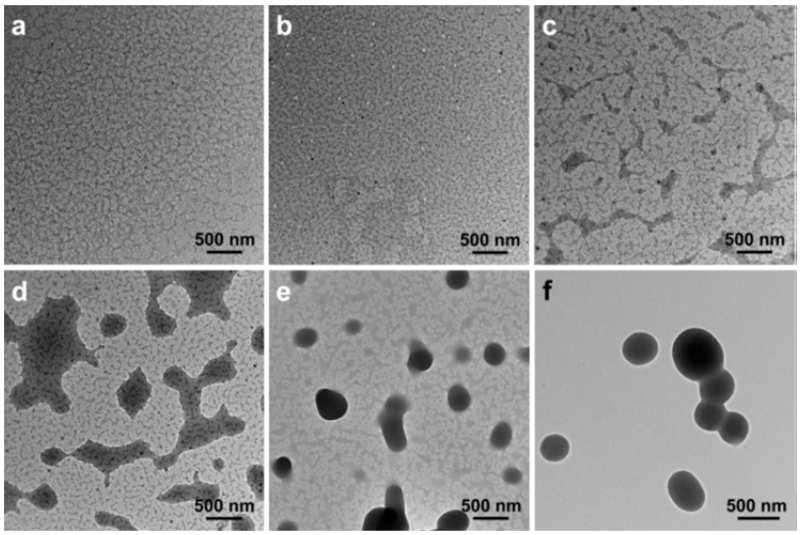

Fig. S37 TEM images of **SS$_{152}$Pt-I** obtained from the chloroform/*n*-hexane solvents with methanol volume ratios of 0% (a), 33% (b), 43% (c), 50% (d), 67% (e), and 75% (f).

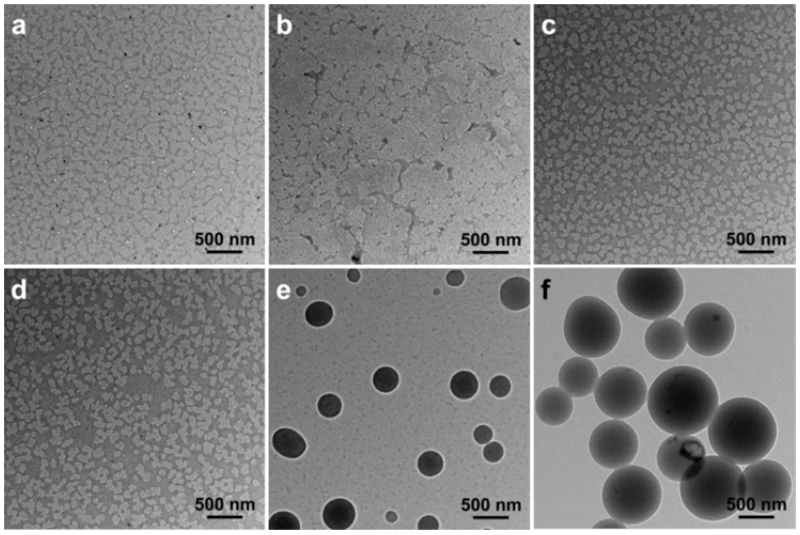

Fig. S38 TEM images of **SS$_{152}$Pt-II** obtained from the chloroform/*n*-hexane solvents with methanol volume ratios of 0% (a), 33% (b), 43% (c), 50% (d), 67% (e), and 75% (f).